



# Synthesis, characterization and antimicrobial activity of nanochitosan and chitosan encapsulated zinc oxide nanoparticles against bacteria and fungus

Sivananthaperumal <sup>1\*</sup>, Thaminum Ansari <sup>1</sup>

<sup>1</sup> PG & Research Department of Chemistry, Muthurangam Govt. Arts College, Vellore, Tamilnadu

\*Corresponding author E-mail: [emiratessiva@gmail.com](mailto:emiratessiva@gmail.com)

## Abstract

In recent years, Nanochitosan and chitosan encapsulated Zinc oxide nanoparticles have gained tremendous attention related to their unique properties such as exhibit antimicrobial properties. On that account, synthesis of nanochitosan and chitosan encapsulated zinc oxide nanoparticles by ionotropic gelation method have fascinating properties such as eco-friendly, biodegradability, biocompatibility, bioactivity, nontoxicity and polycationic nature. Impact of nanochitosan and chitosan encapsulated zinc oxide nanoparticles on biological functions depends on its morphology, particle size, exposure time, concentration, pH, and biocompatibility. They are more effective against microorganisms such as, namely Staphylococcus aureus, E. coli, Salmonella typhimurium, and Klebsiella pneumoniae. In this paper, synthesis of nanochitosan, chitosan encapsulated zinc oxide and compare their potential applications as an antimicrobial agents were discussed. The nanochitosan and chitosan encapsulated zinc oxide nanoparticles have been characterized by Ultraviolet-Visible Spectroscopy (UV), Fourier Transform Infrared Spectroscopy (FT-IR), X-ray Diffraction (XRD), Scanning Electron Microscopy (SEM) were also examined.

**Keywords:** Nanochitosan; Nanoparticles; Zinc Oxide; Encapsulated; Antimicrobial Activity.

## 1. Introduction

In recent years, infectious diseases, specifically those that are caused by microorganism have seen a dramatic proliferation due to resistance to multiple antibiotics, opening the colony by opportunistic pathogens. Nanotechnology has been applied in the development of new antimicrobial therapies, capable of fighting infections caused by pathogens. Nanochitosan and its derivatives are widely explored as functional materials because it has good properties such as biocompatibility, biodegradability and non-toxicity and have wide variety of applications in the development of bioadhesives, nanomaterials, improved drug delivery systems [1], enteric coatings [2] and in medical devices[3 -5].

Nanoparticles based metal oxide properties such as shape, size, roughness and their large surface area, make oxides ideal candidates to interact with bacteria and able to have an antimicrobial effectiveness. Nanosize inorganic compounds have shown remarkable antibacterial activity at very low concentration due to their high surface area to volume ratio and unique chemical and physical features [6]. In addition, these particles are also more stable at high temperature and pressure [7]. It is universally known that zinc oxide nanoparticles are antibacterial and inhibit the growth of microorganisms by permeating into the cell membrane. The oxidative stress damages lipids, carbohydrates, proteins, and DNA [8]. Lipid peroxidation is obviously the most crucial that leads to alteration in cell membrane which eventually disrupt vital cellular functions [9]. It has been supported by oxidative stress mechanism involving zinc oxide nanoparticle against Escherichia coli [10].

Globally, bacterial infections are recognized as serious health issue. New bacterial mutation, antibiotic resistance, outbreaks of pathogenic strains, etc. are increasing, and thus, development of more efficient antibacterial agents is demand of the time. Zinc oxide is known for its antibacterial properties from the time immemorial [11]. In the recent past, antibacterial activity of zinc oxide nanoparticle has been investigated against four known gram-positive and gram-negative bacteria, namely Staphylococcus aureus, E. coli, Salmonella typhimurium, and Klebsiella pneumoniae. The mechanism of interaction of zinc oxide nanoparticles against a variety of microbes has also been discussed in detail. It was observed that the growth-inhibiting dose of the zinc oxide nanoparticles was 15 µg/ml, although in the case of K. pneumoniae, it was as low as 5 µg/ml [12], [13].

The synthesis of Chitosan capped inorganic nanomaterials have been considered as significant antibacterial materials in the clinical field. The results suggested that the synthesized materials can be used in wound dressing applications was reported [14]. Polymer coated metal oxide nanoparticles are cluster of many nanocrystals within a polymer matrix [15].

The bandage collected of composite chitosan hydrogel and ZnO NPs were synthesized and their antimicrobial test indicates that this bandage had strong effects on E. coli and S. aureus, with a highly developed antimicrobial impact on E. coli. [16].

Production and Optimization of Chitosan nanoparticles encapsulated with L-Ascorbic acid and Thymoquinone was completed [17]. The chitosan–copper oxide biopolymer nanocomposites were synthesized and showed significant anti-microbial activity against *Bacillus subtilis*, *Escherichia coli*, *Penicillium notatum* and *Pseudomonas aeruginosa*, assayed using the agar well diffusion method [18]. In this study, we have attempted to chemically modify chitosan into nanochitosan by using ionotropic gelation method and chitosan encapsulated zinc oxide nanoparticles is onto the backbone of nanochitosan. They were characterized by UV, FTIR, TGA, XRD and SEM which elucidated the structural changes in comparison with nanochitosan and regarding chitosan encapsulated zinc oxide nanoparticles as antibacterial and antifungal agent.

## 2. Materials and methods

Chitosan was obtained from Indian sea foods, Cochin, Kerala, India. Sodium tripolyphosphate, zinc oxide, acetic acid and all other chemicals used in the experiments were of analytical grade purchased from Merck, India.

### 2.1. Preparation of nanochitosan

The nanochitosan was prepared by ionotropic gelation method [19] using sodium tripolyphosphate. About 1 g of chitosan was dissolved in 200 ml of 2% acetic acid solution which was prepared using the conductivity water. The above solution was stirred well for 15 minutes. Then to the above prepared chitosan solution and 0.8 g of sodium tripolyphosphate dissolved in 107 ml of conductivity water. The conductivity water was added dropwise upto a milky coloured emulsion like appearance was obtained. This solution was then allowed to settle as suspension by adding conductivity water in excess for 24 hours. After this process is over, the supersaturated solution was then decanted. Then the thick emulsion which was obtained above was then poured into the Petri plates Figure.1 (a).

### 2.2. Preparation of chitosan encapsulated zinc oxide nanoparticles

About 1 g of chitosan was dissolved in 200 ml of 2% acetic acid solution which was prepared using the conductivity water. The above solution was stirred well for 15 minutes. About 1 gram of zinc oxide was added to it and stirred well. Then to the above prepared chitosan solution and 0.8 g of sodium tripolyphosphate dissolved in 107 ml of conductivity water was added. The conductivity water was added drop wise upto a milky coloured emulsion like appearance was obtained. This solution was then allowed to settle as suspension by adding conductivity water in excess for 24 hours. After this process is over, the supersaturated solution was then decanted. Then the thick emulsion which was obtained above was then poured into the Petri plates [20].Figure.1 (b).



Fig. 1: (A): Nanochitosan. (B): Chitosan Encapsulated Zinc Oxide Nanoparticles.

### 2.3. Characterization of nanochitosan and chitosan encapsulated zinc oxide nanoparticles

#### 2.3.1. UV - visible spectroscopy

The absorption spectra of the synthesized Nanochitosan, chitosan encapsulated zinc oxide nanoparticles were characterized by UV-Visible spectroscopy using a double beam spectrophotometer. The Ultraviolet- Visible spectrum was recorded on Hitachi, Model U-2800 Spectrophotometer using acetic acid as a solvent and equipped with a diffuse reflectance attachment for powder samples in between a wavelength scan of 200 and 800 nm.

#### 2.3.2. Fourier transforms infrared spectroscopy (FT-IR)

The synthesized Nanochitosan, Chitosan encapsulated zinc oxide nanoparticles were characterized by using Fourier transform infrared spectroscopy Thermo Nicolet AVATAR 330 spectrophotometer in the range of 4000–400  $\text{cm}^{-1}$  wavelength using KBr pellet, method. The FTIR spectra were normalized and major vibration bands were identified associated with surface functional groups.

#### 2.3.3. Thermo gravimetric analysis (TGA)

TGA analysis was performed to find the relation between weight loss of the synthesized Nanochitosan, Chitosan encapsulated zinc oxide nanoparticles with increasing temperature on a SDT Q600 V 20.9 Build 20 instrument with a heating rate of 20°C/min in nitrogen atmosphere. The weight loss at different stages and the cause for each loss was analyzed.

#### 2.3.4. X-ray diffraction (XRD)

Crystalline structure and the average crystalline size of the synthesized Nanochitosan, Chitosan encapsulated zinc oxide nanoparticles were characterized using X- Ray powder diffract meter (XRD-SHIMADZU XD-D1) using a Ni-filtered  $\text{Cu K}\alpha$  X-ray radiation source.

Debye- Scherer's equation was used to determine the particle size of the samples from  $2\theta$  values. Debye- Scherer's equation:  $D = k\lambda / \beta \cos\theta$

where  $k$ , known as Scherer's constant (shape factor), ranges from 0.9 to 1.0,  $\lambda$  is the wavelength (1.541nm), of the X-Ray radiation source,  $\beta$  is the full width half maximum of the XRD peak (radians) and  $\theta$  is the Bragg's angle.

### 2.3.5. Scanning electron microscope (SEM)

To analyze the morphology, average size and composition, synthesized Nanochitosan, Chitosan encapsulated zinc oxide nanoparticles was characterized by Scanning electron microscope analysis was made using VEGA3 TESCAN SEM machine. Morphology of synthesized samples was characterized by SEM technique at different magnification levels.

### 2.3.6. Antimicrobial studies

The Nano chitosan, Chitosan encapsulated zinc oxide nanoparticles were tested for their antimicrobial activity by agar well diffusion method against pathogenic micro organisms. The three bacterial strains and two fungal strains were used for antimicrobial activity. Two gram negative bacteria (*E. coli* and *Salmonella typhi*) and One gram positive bacteria (*Staphylococcus aureus*) were used. The fungal strains such as *Aspergillus Niger* and *Aspergillus flavus* were tested by agar well diffusion method according to the procedures reported [20].

#### Antibacterial Assay

The sterilized medium was poured into a Petri dish in a uniform thickness and kept a side for solidification. Using sterilized swabs, even distribution of lawn culture was prepared using test bacteria such as *Escherichia coli*, *Staphylococcus aureus* and *Salmonella typhi* in Muller Hinton Agar (MHA) plates. Muller Hinton Agar was prepared and sterilized. 20 ml of media was poured in Petri plates and allowed for solidification. The bacterial lawn culture was made using sterile cotton swab and labeled. The wells were made in the media with the help of a metallic borer with centers at least 24 mm. Recommended concentration  $10^{-3}$  M of test nanochitosan, chitosan encapsulated zinc oxide nanoparticles in acetic acid were introduced in the respective wells. Other wells were supplemented with reference antibacterial drug.

#### Antifungal Assay

The antifungal activities of nanochitosan and chitosan encapsulated zinc oxide nanoparticles were studied against two fungal cultures, *Aspergillus Niger* and *Aspergillus flavus*. Sabouraud dextrose agar was prepared, sterilized and prepare the culture plates same like Muller Hinton Agar. After solidification of media, respective fungal spore suspensions were transferred to Petri plates. The wells were made in the media with the help of a sterile metallic borer with centers at least 24 mm. Recommended concentration  $10^{-3}$  M of nanochitosan, nanochitosan, nanochitosan encapsulated zinc oxide and chitosan encapsulated zinc oxide nanoparticles in acetic acid were introduced in the respective wells. The plates were incubated immediately at 72 h. The results were recorded as zones of complete inhibition (mm). Growth inhibition was compared with standard antibiotic Amphotericin B used as positive control.

## 3. Results and discussion

### 3.1. UV – VIS spectra

The UV-Vis absorbance spectra of purified Nanochitosan, and Chitosan encapsulated ZnO nanoparticles are shown in Figure. 3.1 (a) and 3.1 (b). As observed in the literature, Chitosan sample did not show much absorbance in the wavelength range from 200 nm to 800 nm due to lack of conjugated double bonds in the structure [21]. Broad absorption bands observed at 200 and 322 nm could be related to the CO group [22]. In Nanochitosan and Chitosan encapsulated ZnO nanoparticles the peak observed at 280 nm correspond to the interactions between nanochitosan and ZnO nanoparticles.

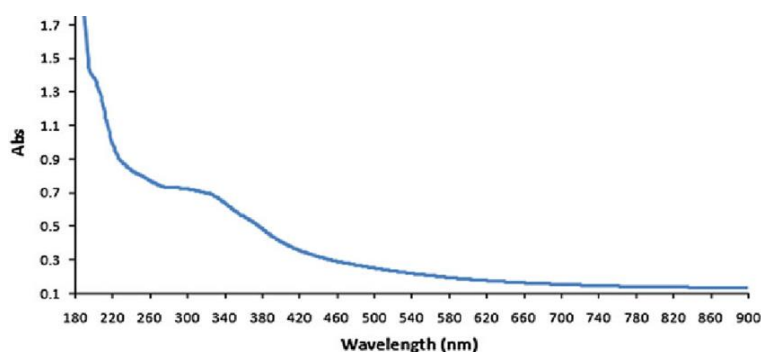


Fig. 3.1: (A). UV Spectra of Nanochitosan.

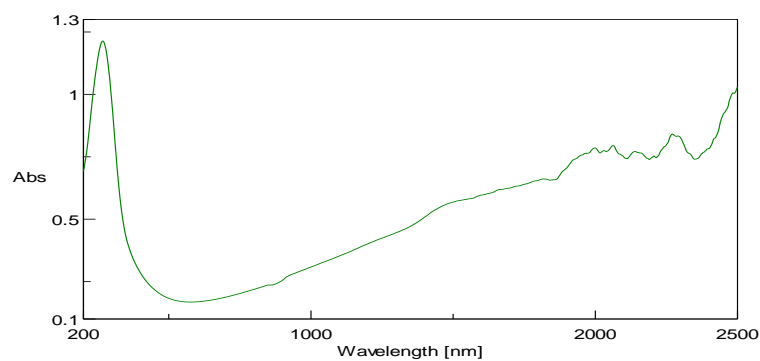


Fig. 3.2: (B). UV Spectra of Chitosan Encapsulated ZnO NP'S.

### 3.1.1. FT-IR spectra of nanochitosan

The FT-IR spectra of nanochitosan as shown in Figure 3.2 (a) and Table 3.1 which was obtained from chitosan by ionotropic gelation method showed some different bands. It is remarkable that in the case of nanochitosan, a strong peak was obtained at  $3236.55\text{ cm}^{-1}$ ,  $2864.29\text{ cm}^{-1}$ ,  $1631.78\text{ cm}^{-1}$ ,  $1143.79\text{ cm}^{-1}$  and  $1064.71\text{ cm}^{-1}$  which indicates the presence of intermolecular hydrogen bonded NH stretching, asymmetrical and symmetrical CH stretching in  $\text{NH}_3^+$ , C=O stretching, OH of (O=P-OH) P=O stretching and P-O stretching and C-O-C linkage and  $896.90\text{ cm}^{-1}$  indicate the presence of -NH bending, respectively [23].

The shift of the peak observed at  $3454.75\text{ cm}^{-1}$  corresponding to the presence of NH, OH stretching in chitosan to lower wave number ( $3236.55\text{ cm}^{-1}$ ) in nanochitosan samples may indicate an interaction of the sodium tripolyphosphate with the pure chitosan. The above observed results showed that the  $\text{CONH}_2$  and  $\text{NH}_2$  groups of chitosan are both slightly cross-linked with a sodium polyphosphate molecule. In addition to this also the appearance of some new peaks in nanochitosan when compared to the pure chitosan which concludes that the nanochitosan was formed from the pure chitosan.

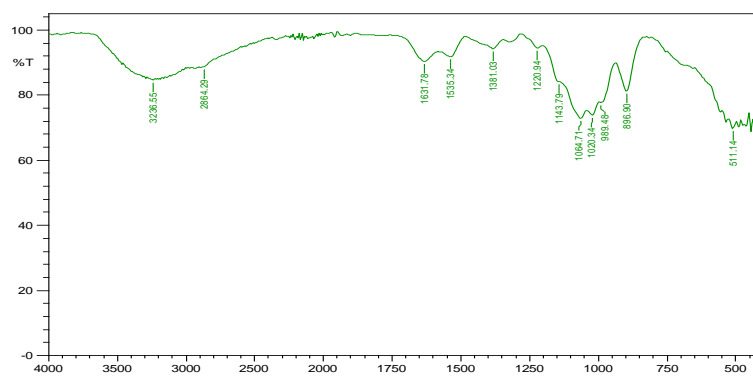


Fig. 3.2: (A). FT-IR Spectra of Nanochitosan.

### 3.1.2. FT-IR spectrum of chitosan encapsulated zinc oxide nanoparticles

The IR spectra of Chitosan encapsulated ZnO nanoparticles showed a prominent peak at  $3242.34\text{ cm}^{-1}$  corresponds to -OH stretching of axial OH group and -NH stretching Figure- 3.2 (b) and Table 3.1. A peak at  $2920.23\text{ cm}^{-1}$  was due to aliphatic -CH asymmetric stretching, strong peak obtained at  $1629.85\text{ cm}^{-1}$  indicate the presence of C=O in amide group, and  $1062.78\text{ cm}^{-1}$  indicate the presence of C-O-C stretching of glycosides linkage and  $893.04\text{ cm}^{-1}$  indicate the presence of -NH bending, respectively [24]. Appearance of new peaks at  $1219.01\text{ cm}^{-1}$  and  $1018.41\text{ cm}^{-1}$  corresponds to P=O stretching, P-O stretching respectively was due to the interaction of sodium tripolyphosphate with chitosan and confirms the conversion of chitosan to nanochitosan.

The shift of the peaks observed at  $3242.34\text{ cm}^{-1}$  to lower wave number in nanochitosan indicate cross linking had taken place effectively between sodium tripolyphosphate and chitosan. The characteristic peak for Zn-O group is located at  $630.72\text{ cm}^{-1}$  is due to the attachment of amide group and stretching mode of ZnO [25]. In addition to these results, the characteristic peaks of (Figure -2.2(b)) are shifted to lower wave number, the wide peak at  $3454.75\text{ cm}^{-1}$ , corresponding to the stretching vibration of hydroxyl, amino and amide groups, moved to lower wave numbers  $3242.34\text{ cm}^{-1}$ , and became broader and stronger, which indicated the strong interaction between these groups and ZnO [26], compared with (Figure-2.2(a)), a point which could be explained in terms of strong attachment of ZnO to the amide groups of chitosan molecules.

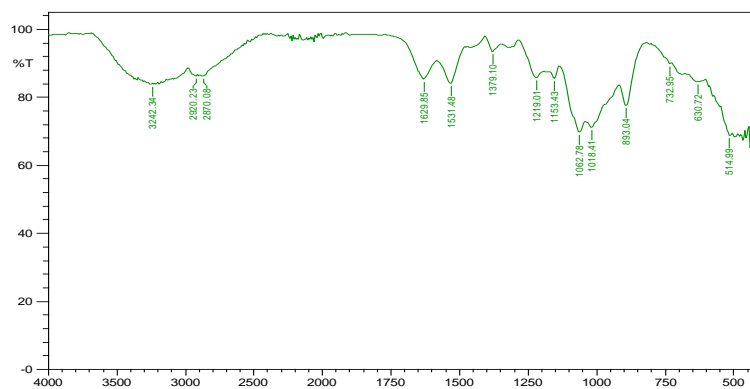


Fig. 3.2: (b). FT-IR Spectra of Chitosan Encapsulated Zinc Oxide NP's.

Table 3.1: FT-IR Spectral Details of Nanochitosan Encapsulated Zinc Oxide and Chitosan Encapsulated Zinc Oxide Nanoparticles

Samples	$\approx \nu \text{ cm}^{-1}$ H bond N-H and OH str	$\approx \nu \text{ cm}^{-1}$ CH str	$\approx \nu \text{ cm}^{-1}$ C=O in amide	$\approx \nu \text{ cm}^{-1}$ P=O str	$\approx \nu \text{ cm}^{-1}$ C-O-C linkage	$\approx \nu \text{ cm}^{-1}$ N-H bending	$\approx \nu \text{ cm}^{-1}$ ZnO
Nano Chitosan	3236.55	2864.29	1631.78	1143.79	1064.71	896.90	-
Chitosan + ZnO NP's	3242.34	2920.23	1629.85	1219.01	1062.78	893.04	630.72

### 3.2. Thermo gravimetric analysis of nanochitosan

TGA is the method for studying thermal stability of polymers. Three weight losses are observed in nanochitosan curve. TGA thermogram of nanochitosan as shown in Figure 3.3(a) designate that the first thermal incident occurs at temperature range 50-150°C with a weight loss of 8% to 10% which may be owing to the loss of residual water there in the sample. The further weight losses at 300-400°C is due to the degradation of chitosan [27]. Nanochitosan starts by a disorderly splitting of the glycosidic bonds followed by a further decomposition to acetic, butyric and lower fatty acids. The second stage starts at the range of 170-370°C. The third stage starts at the range of 500-600°C. The thermal deprivation of nanochitosan upto 800°C shows that around 45.63% of the sample remained as deposit at the end of the experiment shows high thermal stability of nanochitosan.

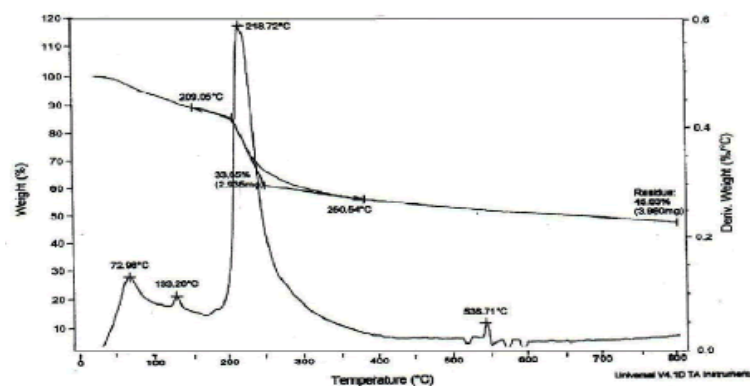


Fig. 3.3: (A) TGA of Nanochitosan.

#### 3.2.1. Thermo gravimetric analysis of chitosan encapsulated zinc oxide nanoparticles

TGA details of nanochitosan encapsulated zinc oxide as shown in Figure 3.3 (b). TGA thermogram of nanochitosan loaded zinc oxide designate that the first thermal decomposition occurs at temperature range 30-210°C with a weight loss from 8% to 9% is 18.24% which may be owing to the loss of residual water present in the sample. The second decomposition starts at 220°C and ends at 510°C. The weight loss is 29.51% this may be owing to the thermal and oxidative decomposition of the sample [28]. The third stage of disintegration starts at 510°C to 800°C. The weight loss is 2.277%. At the finish of the experiment nearly 49.90% of the sample remained as deposit showing the higher thermal stability of chitosan encapsulated zinc oxide.

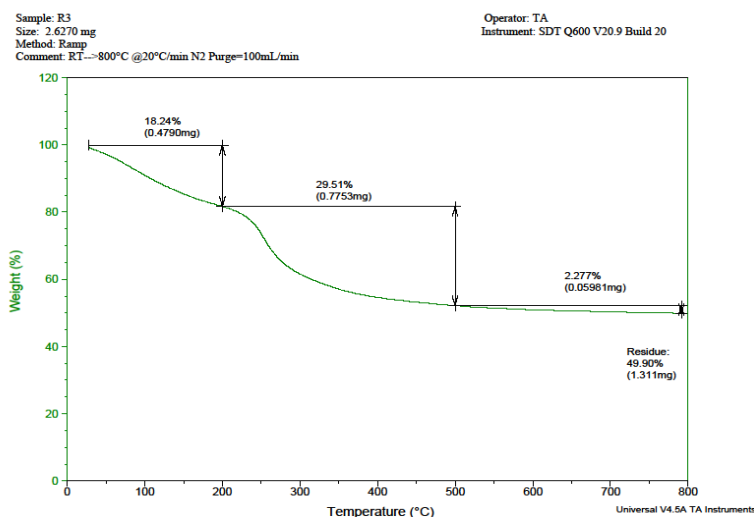


Fig. 3.3: (b) TGA of Chitosan Encapsulated Zinc Oxide NPs.

### 3.3. XRD spectra of nanochitosan

The XRD pattern of nanochitosan Figure 3.4 (a) showed at  $2\theta=18^\circ$  and  $20^\circ$ . The XRD  $2\theta$  values at  $10^\circ$  and  $20^\circ$  of nanochitosan were disappearing or merging to give the broad peak at  $18.86^\circ$  during the formation of nanochitosan. The appearance of broad peak in nanochitosan may be due to the increase in packing of the chitosan chains by the ionic cross-linking which can deform the crystalline regions. In addition to this, the weakening of the rigid crystalline nature of chitosan after cross-linking may also be due to the destruction of  $\text{NH}_2$  groups present in the glucosamine units in chitosan due to hydrogen bonding. These obtained results indicated that there was an effective cross-linking, molecular miscibility and also certain interaction takes place between the chitosan with ionic cross linking agent. Thus the XRD pattern of nanochitosan is characteristic of an amorphous polymer [22]. XRD patterns of nanochitosan showed a number of Bragg's diffraction peaks at  $2\theta$  of 21.38, 23.80, 26.47, 51.35.

The average particle size of the nanochitosan was calculated from the four most intense peak using Debye - Scherer's equation.

$$D = K \lambda / \beta \cos \Theta$$

where,  $K$  is known as Scherer's contact [shape factor], range from 0.9 to 1.0,  $\lambda$  is the wavelength (1.541 nm) of the X-ray radiation source,  $\beta$  is the full width half maximum of the XRD peak (radians) and  $\Theta$  is the Bragg's angle. The average particle size of the Nanochitosan was 24.7487 nm Table 3.2.

Table 3.2: Determination of the Average Particle Size of the Nanochitosan

S. No	$2\theta$ (Degrees)	FWHM (Degrees)	$B = \pi * \text{FWHM} / 180$ (radians)	$D = K\lambda / \beta \cos\theta$ (nm)
1	21.38	0.279	0.0048	30.0389
2	23.80	0.218	0.0038	34.0929
3	26.47	0.287	0.0050	23.3131
4	51.35	0.299	0.0052	11.5517
Average particle size				24.7487

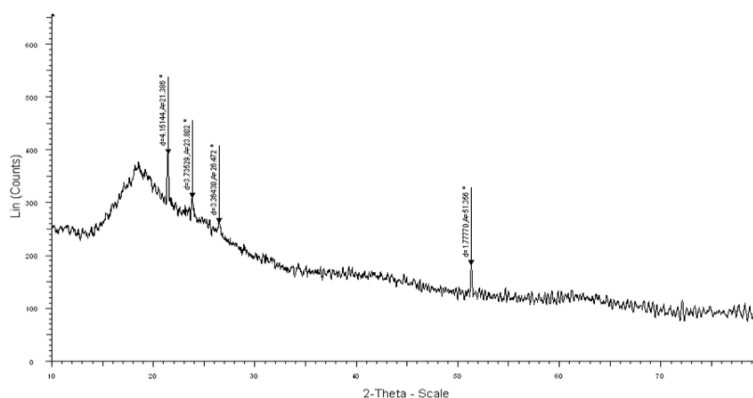


Fig. 3.4: (A) XRD of Nanochitosan.

#### 3.3.1. XRD spectra of chitosan encapsulated zinc oxide nanoparticles

XRD Pattern of Chitosan encapsulated with Zinc Oxide nanoparticles as shown in Figure 3.4 (b), the spectra showed well defined distinctive peak at  $2\theta$  value of the broadening of the peak was due to the amorphous, nature of the chitosan / ZnO polymer by the ionic cross-linking at TPP with chitosan which can deform the crystalline structure of chitosan.

XRD Patterns of chitosan encapsulated with Zinc oxide nanoparticles showed a number of Bragg's diffraction peaks at  $2\theta$  of 28.20, 36.21, 39.72, 49.12, 53.58, 56.40. The Average particle size of the chitosan / ZnO NP's was calculated from the six most intense peak using Debye-Scherer's equation.

$$D = K \lambda / \beta \cos \Theta$$

Where,  $k$  is known as scherer's contact [shape factor], range from 0.9 to 1.0,  $\lambda$  is the wavelength (1.541 nm) of the X-ray radiation source,  $\beta$  is the full width half maximum of the XRD peak (radians) and  $\Theta$  is the Bragg's angle. The average particle size of the chitosan encapsulated Zinc Oxide Nanoparticles was 32.9757 nm Table 3.3.

**Table 3.3:** Determination of the Average Particle Size of the Chitosan Encapsulated Zinc Oxide Nanoparticles

S. No	$2\theta$ (Degrees)	FWHM (Degrees)	$B=\pi*FWHM/180$ (radians)	$D=K\lambda/\beta \cos\theta$ (nm)
1	28.20	0.0034	0.0479	32.1711
2	36.21	0.0017	0.0307	50.1954
3	39.72	0.0033	0.0655	23.5267
4	49.12	0.0030	0.0736	20.9375
5	53.58	0.0027	0.0723	21.3139
6	56.40	0.0011	0.0310	49.7096
Average particle size				32.9757

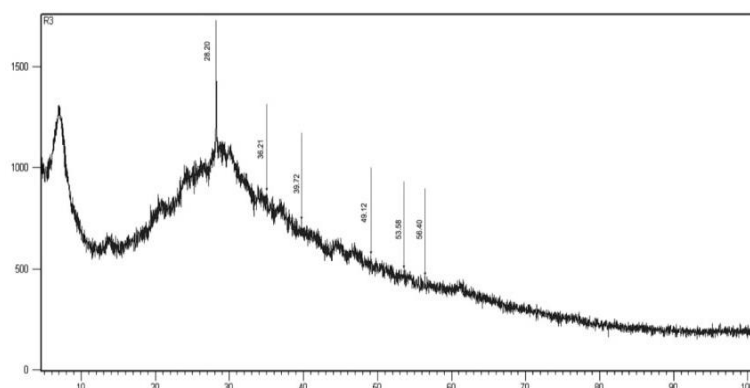


**Fig. 3.4:** (B). XRD of Chitosan Encapsulated Zinc Oxide NP'S.

### 3.4. SEM analysis of nanochitosan

The surface morphology of the synthesized Nanochitosan was examined using SEM. The SEM image was taken at different magnification including X 1,500, X 5000, and X 10,000 worked at 20 keV accelerating voltage. Figure 3.5 (a) showed the SEM images of synthesized chitosan nanoparticles. The images reveal the agglomerated nanoparticles. The image shows the size of nanoparticles in the range of 181nm.

Similarly [29] reported that the prepared chitosan NPs was microporous structured uneven shape and agglomerated. The TPP concentration exceeds 1 %, the chitosan aggregation was formed and precipitated. It may be due to more chitosan chains were cross linked in the presence of high concentration of TPP. The diameter of the chitosan-TPP nanoparticles increased with increase of TPP [30].

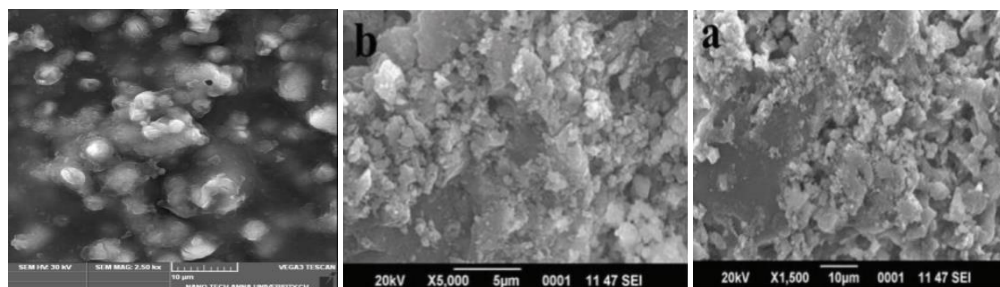


**Fig. 3.5:** (A) SEM Images of Nanochitosan.

#### 3.4.1. SEM analysis of chitosan encapsulated zinc oxide nanoparticles

The surface morphology of chitosan encapsulated zinc oxide nanoparticles films was evaluated using scanning electron microscope. The SEM images was taken at different magnification of x 2000, x 10,000 and x 50,000. In the SEM photographs, presence of nanochitosan with zinc oxide particles on the polymer surface was spotted as white coloured images. The surface of nanochitosan is film is rather smooth, compact and homogenous, whereas in films, the incorporation of nanoparticles (ZnO) modified the chitosan surface to coarse and heterogeneous. Thin films of the samples were prepared by dropping a very small amount of the sample on glass plates and then allowed to dry at room temperature. Figure 3.5 (b) showed the SEM images of synthesized chitosan encapsulated zinc oxide nanoparticles.

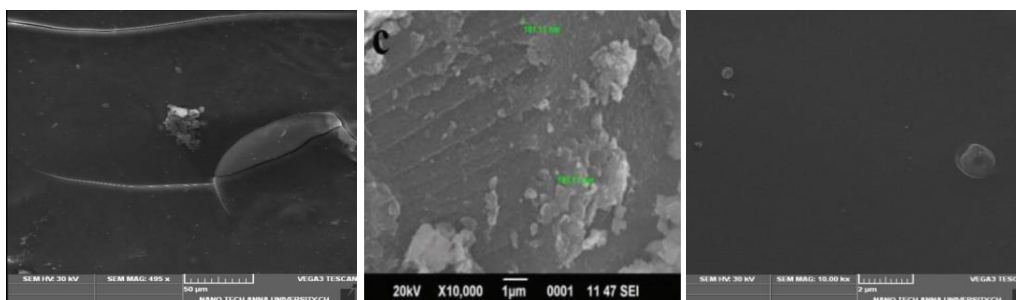


Fig. 3.5: (B). SEM Images of Chitosan Encapsulated Zinc Oxide NP's.

### 3.5. Antimicrobial activity of chitosan encapsulated zinc oxide NP'S

The antibacterial activity of synthesized Chitosan encapsulated Zinc Oxide NP's was investigated against selected pathogens such as *Staphylococcus aureus*, *E. coli*, *Salmonella typhimurium*, and *Klebsiella pneumoniae*. by using the agar well diffusion method and the result as shown in Table 3.6 (a). In general, the synthesized of nanochitosan and chitosan encapsulated Zinc Oxide NP's by using ionotropic gelation method exhibited strong antibacterial activity against gram negative bacteria (*E. coli* and *Salmonella typhi*) and gram positive bacteria (*Staphylococcus aureus*) bacteria strains. Similarly the fungal strains such as *Aspergillus Niger* and *Aspergillus flavus* were tested by agar well diffusion method and the result as shown in Table 3.6 (b). Further, the result of antibacterial and antifungal activity clearly indicated that chitosan encapsulated zinc oxide NP's in all concentration ranges showed a greater zone of inhibition against all bacterial and fungal strains compared to nanochitosan. This may be due to the small crystal size and the synergetic antibacterial activity of the chitosan encapsulated zinc oxide NP's [31-33]. Ciprofloxacin was used as reference antibacterial agent. Furthermore, the chitosan encapsulated zinc oxide NP's showed better antibacterial activity against gram-positive and gram-negative bacterial strains.

Similarly fungal plates were incubated at room temperature for 48 h. Antifungal activity was evaluated by measuring the diameter of the zone of inhibition in mm against the test microorganisms such as *Aspergillus Niger* and *Aspergillus flavus* with the solvent DMSO was used as solvent control and Amphotericin B was used as reference.

Table 3.6: (A). Antibacterial Activity of Chitosan Encapsulated Zinc Oxide NP's

S. No.	Microorganisms	Zone of inhibition in mm			
		Control	R1	R2	Ciprofloxacin
1.	<i>Escherichia coli</i>	-	10	17	18
2.	<i>Salmonella typhi</i>	-	13	10	25
3.	<i>Klebsiella pneumoniae</i>	-	25	25	18
4.	<i>Enterococcus faecalis</i>	-	12	10	30
5.	<i>Bacillus subtilis</i>	-	12	13	30
6.	<i>Staphylococcus aureus</i>	-	10	11	20

R1 – Nanochitosan

R2 -Chitosan encapsulated Zinc oxide NPs

Table 3.6: (B). Antifungal Activity of Chitosan Encapsulated Zinc Oxide NP's

S. No	Microorganisms	Zone of inhibition in mm			Amphotericin-B
		Control	R1	R2	
1.	<i>Candida albicans</i>	-	12	11	15
2.	<i>Aspergillus niger</i>	-	13	13	10
3.	<i>Aspergillus flavus</i>	-	15	30	10

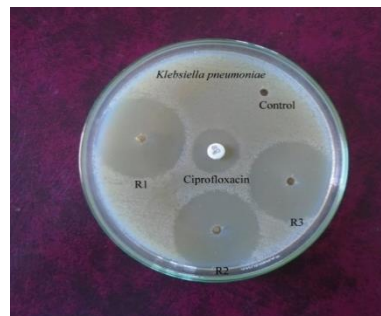
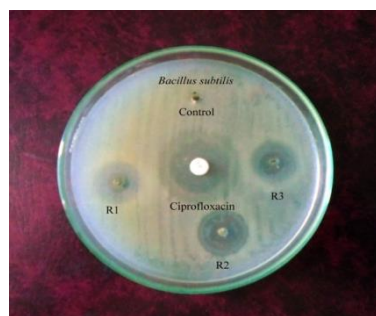
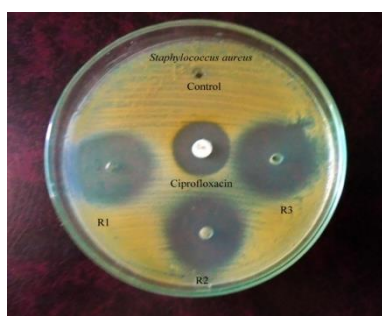




Fig. 3.6: (A). Antibacterial Images of Nanochitosan and Chitosan Encapsulated Zinc Oxide Nanoparticles.

Table 3.6: (b). Antifungal Activity of Chitosan encapsulated Zinc Oxide NP's

S. No	Microorganisms	Zone of inhibition in mm			
		Control	R1	R2	Amphotericin-B
1.	<i>Candida albicans</i>	-	12	11	15
2.	<i>Aspergillus niger</i>	-	13	13	10
3.	<i>Aspergillus flavus</i>	-	15	30	10

R1 – Nanochitosan

R2 -Chitosan encapsulated Zinc oxide NPs



Fig.3.6: (B): Antifungal Images of Nanochitosan and Chitosan Encapsulated Zinc Oxide Nanoparticles.

## 4. Conclusions

In this study, Nanochitosan and Chitosan encapsulated Zinc oxide NP's were successfully synthesized by using ionotropic gelation method. They were characterized by using techniques such as TGA, XRD, SEM, FTIR, and UV-Vis. From the TGA analysis, the synthesized nanochitosan and chitosan encapsulated Zinc oxide NP's showed thermal stability above 400°C. The crystallinity of the synthesized nanochitosan and chitosan encapsulated Zinc oxide NP's was proved from XRD analysis, and the analysis results showed that there was an effective cross-linking, molecular miscibility and also certain interaction takes place between the chitosan with ionic cross linking agent. Thus the XRD pattern of nanochitosan is characteristic of an amorphous polymer. XRD patterns of nanochitosan showed a number of bragg's diffraction peaks at  $2\theta$  of 21.38,23.80,26.47,51.35 and XRD patterns of chitosan encapsulated with Zinc oxide nanoparticles showed a number of Bragg's diffraction peaks at  $2\theta$  of 28.20,36.21,39.72,49.12,53.58,56.40. All the diffraction peaks fit well with the crystalline structure. SEM analysis showed that the morphology of the synthesized nanochitosan and chitosan encapsulated Zinc Oxide NP's were predominantly crystalline even though nanorod-shaped structures were also observed. Further, the synthesized nanochitosan and chitosan encapsulated Zinc Oxide NP's have proved themselves to be strong antibacterial agent against *E. coli* and *Salmonella typhi*, and *Staphylococcus aureus* strains. Similarly, antifungal activity against strains such as *Aspergillus Niger* and *Aspergillus flavus* were observed..

## References

- [1] A. Agnihotri, Sunil, N. Mallikarjuna, Nadagouda and M. Aminabhavi, Tejraj, "Recent advances on chitosan-based micro- and nanoparticles in drug delivery". *Journal of Controlled Release*, 2004, 100 (1):528. <https://doi.org/10.1016/j.jconrel.2004.08.010>.
- [2] K.M. Aiedeh, M.O.Taha and H. Al-Khatib, "Evaluation of chitosan succinate and chitosan phthalate as enteric coating polymers for diclofenac sodium tablets". *Journal of Drug Delivery Science and Technology*, 2005, 15 (3): 207–211. [https://doi.org/10.1016/S1773-2247\(05\)50033-9](https://doi.org/10.1016/S1773-2247(05)50033-9).
- [3] S.K. Shukla, A.K. Mishra, O.A. Arotiba and B.B. Mamba, "Chitosan-based nanomaterials: A state-of-the-art review". *International Journal of Biological Macromolecules*, 2013, 59: 46–58. <https://doi.org/10.1016/j.ijbiomac.2013.04.043>.
- [4] J.H. Ryu, S. Hong, H. Lee, "Bio-inspired adhesive catechol-conjugated chitosan for biomedical applications: A mini review". *Acta Biomaterialia*, 2015, 27: 101–115. <https://doi.org/10.1016/j.actbio.2015.08.043>.
- [5] M.Z. Elsabee, E.S. Abdou, "Chitosan based edible films and coatings: A review". *Materials Science and Engineering: C*, 2013, 33 (4): 1819–41. <https://doi.org/10.1016/j.msec.2013.01.010>.
- [6] M. Rai, A. Yadav, A. Gade, Silver nanoparticles as a new generation of antimicrobials. *Biotechnol Adv* ,2009,27:76–83 <https://doi.org/10.1016/j.biotechadv.2008.09.002>.
- [7] J. Sawai, Quantitative evaluation of antibacterial activities of metallic oxide powders (ZnO, MgO and CaO) by conductimetric assay. *J Microbiol Methods*, 2003, 54:177–182 [https://doi.org/10.1016/S0167-7012\(03\)00037-X](https://doi.org/10.1016/S0167-7012(03)00037-X).
- [8] C.J. Frederickson, J.Y. Koh, A.L. Bush, The neurobiology of zinc in health and disease. *Na Rev Neurosci* ,2005,6:449–462 <https://doi.org/10.1038/nrn1671>.
- [9] S.A. Kelly, C.M. Havrilla, T.C. Brady, K.H. Abramo, E.D. Levin, Oxidative stress in toxicology: established mammalian and emerging piscine model systems. *Environ Health Perspect* ,1998,106:375–384 <https://doi.org/10.1289/ehp.98106375>.
- [10] L.E. Rikans, K.R. Hornbrook, Lipid peroxidation, antioxidant protection and aging. *Biochim Biophys Acta* ,1997,1362:116–127 [https://doi.org/10.1016/S0925-4439\(97\)00067-7](https://doi.org/10.1016/S0925-4439(97)00067-7).
- [11] L. Zhang, Y. Jiang, Y. Ding, M. Povey, D. York , Investigation into the antibacterial behaviour of suspensions of ZnO nanoparticles (ZnO nanofluids). *J Nanopart Res*,2007 9:479–489 <https://doi.org/10.1007/s11051-006-9150-1>.
- [12] R. Brayner, R. Ferrari-Iliou, N. Brivois, S. Djediat, M.F. Benedetti, F.Fiévet, Toxicological impact studies based on Escherichia coli bacteria in ultrafine ZnO nanoparticles colloidal medium. *Nano Lett*, 2006, 6:866–870 <https://doi.org/10.1021/nl052326h>.
- [13] P.K. Stojmenov, R.L. Klinger, G.L. Marchin, K.J. Klabunde, Metal oxide nanoparticles as bactericidal agents. *Langmuir*,2002,18:6679–6686 <https://doi.org/10.1021/la0202374>.
- [14] Tippabattini Jayaramudu et al. Chitosan capped copper oxide/ copper nanoparticles encapsulated microbial resistant nanocomposite films, *International Journal of Biological Macromolecules*, 2019. <https://doi.org/10.1016/j.ijbiomac.2019.01.145>.
- [15] M. Erik Shapiro, "Biodegradable, polymer encapsulated, metal oxide particles for MRI-based cell tracking". *Magn Reson Med*, 2015, 73(1): 376–389. <https://doi.org/10.1002/mrm.25263>.
- [16] Vu Khac Hoang Bui, Duckshin Park, Young-Chul Lee, Virginia Gómez, Silvia Irusta. "Chitosan Combined with ZnO, TiO<sub>2</sub> and Ag Nanoparticles for Antimicrobial Wound Healing Applications: A Mini Review of the Research Trends". *Polymers*, 2017, 9(1):21. <https://doi.org/10.3390/polym9010021>.
- [17] Nurhanisah Othman et al. Synthesis and Optimization of Chitosan Nanoparticles Loaded with L-Ascorbic Acid and Thymoquinone, *nanomaterials*, 2018. <https://doi.org/10.3390/nano8110920>.
- [18] S.Logpriya et al. Preparation and characterization of ascorbic acid-mediated chitosan-copper oxide nanocomposite for anti-microbial, sporicidal and bio-film-inhibitory activity, *Journal of Nanostructure in Chemistry*, 2018. <https://doi.org/10.1007/s40097-018-0273-6>.
- [19] K.G.H. Desai, C. Liu, H.J. Park, Microencapsulation, 2006, 23, 79-90. <https://doi.org/10.1080/02652040500435360>.
- [20] K. Kataoka, T. Matsumoto, M. Tokohama, T. Okano, Y. Sakurai, *J. Controlled Release*. 2000, 64, 143-153. [https://doi.org/10.1016/S0168-3659\(99\)00133-9](https://doi.org/10.1016/S0168-3659(99)00133-9).
- [21] Subhani Bandara , Codi-anne Carnegie , Chevaun Johnson , Feyisayo Akindoju , Ebonee Williams , Julia M. Swaby , Aderemi Oki , Laura E. Carson. Synthesis and characterization of Zinc/Chitosan-Folic acid complex, *Heliyon*, 2018. <https://doi.org/10.1016/j.heliyon.2018.e00737>.
- [22] Sedigheh Vaezifar, Shahnaz Razavi, Mohammad Ali Golozar, Saied Karbasi, Mohammad Morshed, Mahdi Kamali. Effects of Some Parameters on Particle Size Distribution of Chitosan Nanoparticles Prepared by Ionic Gelation Method. *Journal of cluster science*. 2013,24:891-903 <https://doi.org/10.1007/s10876-013-0583-2>.
- [23] S.T. Lee, F.L. Mi, Y.J. Shen, S.S. Shyu, *Polymer*, 2001, 42, 1879-1892 [https://doi.org/10.1016/S0032-3861\(00\)00402-X](https://doi.org/10.1016/S0032-3861(00)00402-X).
- [24] P.N. Sudha, K.Rajeshwari, Srinivasan Latha, T.Gomathi, Sangeetha. "Preparation and Characterisation study of Nanochitosan (NCS) and polyvinyl alcohol (PVA) binary blends with glutaraldehyde as a crosslinking agent", 2016.
- [25] Gui-Yin Li, Yu-Ren Jiang, Ke-long Huang, P. Ding, Jie Chen. "Preparation and properties of magnetic Fe<sub>3</sub>O<sub>4</sub>-chitosan nanoparticles". *Journal of Alloys and Compounds*, 2008, 466:451–456 <https://doi.org/10.1016/j.jallcom.2007.11.100>.
- [26] M.M. AbdElhady, "Preparation and Characterization of Chitosan / Zinc Oxide Nanoparticles for Imparting Antimicrobial and UV Protection to Cotton Fabric". *International Journal of Carbohydrate Chemistry*, 2012, Article ID 840591, 6 pages. <https://doi.org/10.1155/2012/840591>.
- [27] S. Singh et al. Relative contributions of cystathionine beta-synthase and gamma-cystathionase to H<sub>2</sub>S biogenesis via alternative trans-sulfuration reactions. *Journal of Biological Chemistry*, 2009, 284(33):22457-66. <https://doi.org/10.1074/jbc.M109.010868>.
- [28] Esra BILGIN SIMSEK "Investigation of photocatalytic Activity of chitosan/ Poly (vinylalcohol)/ TiO<sub>2</sub>/ Boron Nanocomposites". *Journal of Natural and Applied Sciences*, 2017. <https://doi.org/10.19113/sdufbed.57694>.
- [29] Qi L, Xu Z, Jiang X, Hu C, Zou X, Preparation and antibacterial activity of chitosan nanoparticles, *Carbohydrate Research*,2004,339:2693-2700. <https://doi.org/10.1016/j.carres.2004.09.007>.
- [30] Jiayin Zhao and Jianmin Wu, Preparation and Characterization of the Fluorescent Chitosan Nanoparticle Probe, *Chinese Journal of Analytical Chemistry*, 2006, 34(11):1555-1559. [https://doi.org/10.1016/S1872-2040\(07\)60015-2](https://doi.org/10.1016/S1872-2040(07)60015-2).
- [31] C. Perez, M. Pauli, P. Bazerque, An antibiotic assay by the agar-well diffusion method. *Acta Biologica ET Medicinae Experimentalis*, 1990, 15:13-115.
- [32] N. Erdemog lu, E. Ku Peli, E. Yes, R. Ilada, Anti-inflammatory and antinociceptive activity assessment of plants used as remedy in Turkish folk medicine. *Journal of Ethnopharmacol*, 2003, 89:123-1. [https://doi.org/10.1016/S0378-8741\(03\)00282-4](https://doi.org/10.1016/S0378-8741(03)00282-4).
- [33] C.F. Bagamboula, M. Uyttendaele, J. Debevere, Inhibitory effect of thyme and basil essential oils, carvacrol, thymol, estragol, linalool and p-cymene towards *Shigella sonnei* and *S. flexneri*, *Food Microbiology*,2004,21:33-42. [https://doi.org/10.1016/S0740-0020\(03\)00046-7](https://doi.org/10.1016/S0740-0020(03)00046-7).